

## Lasing behaviors upon phase transition in solution-processed perovskite thin films

Tsung Sheng Kao, Yu-Hsun Chou, Chun-Hsien Chou, Fang-Chung Chen, and Tien-Chang Lu

Citation: [Applied Physics Letters](#) **105**, 231108 (2014); doi: 10.1063/1.4903877

View online: <http://dx.doi.org/10.1063/1.4903877>

View Table of Contents: <http://scitation.aip.org/content/aip/journal/apl/105/23?ver=pdfcov>

Published by the [AIP Publishing](#)

---

### Articles you may be interested in

[Random lasing from localized modes in strongly scattering systems consisting of macroporous titania monoliths infiltrated with dye solution](#)

Appl. Phys. Lett. **97**, 031118 (2010); 10.1063/1.3464962

[Laser operation in nondoped thin films made of a small-molecule organic red-emitter](#)

Appl. Phys. Lett. **95**, 033305 (2009); 10.1063/1.3182820

[Optical gain at 1535 nm in LaF<sub>3</sub>:Er, Yb nanoparticle-doped organic-inorganic hybrid material waveguide](#)

Appl. Phys. Lett. **91**, 161109 (2007); 10.1063/1.2799582

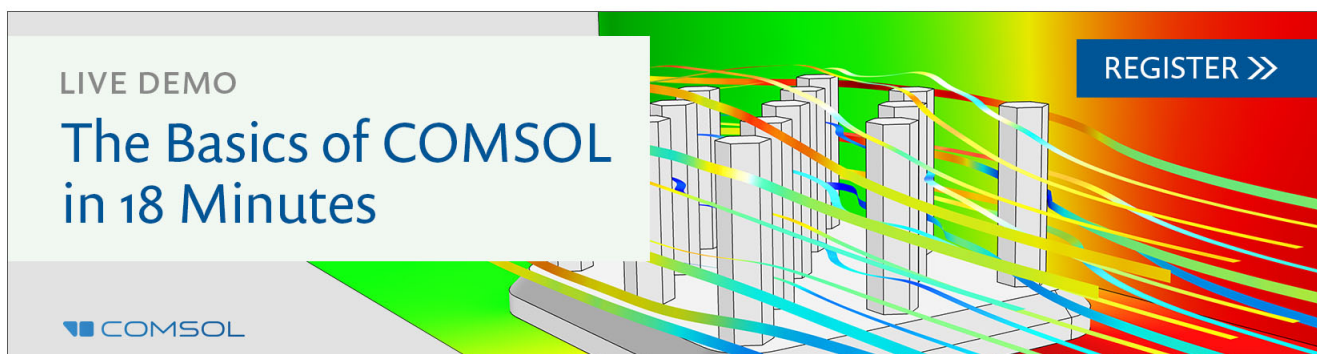
[Demonstration of optical gain at 1.06 μm in a neodymium-doped polyimide waveguide](#)

Appl. Phys. Lett. **77**, 1253 (2000); 10.1063/1.1290157

[Reversible optical control of transmittance in polymer/liquid crystal composite films by photoinduced phase transition](#)

J. Appl. Phys. **86**, 5927 (1999); 10.1063/1.371717

---

A promotional banner for COMSOL software. It features a 3D visualization of a waveguide structure with colorful light rays passing through it. The text 'LIVE DEMO' is in the top left, 'The Basics of COMSOL in 18 Minutes' is in the center, and 'REGISTER >>' is in a blue button in the top right. The COMSOL logo is in the bottom left.

LIVE DEMO

# The Basics of COMSOL in 18 Minutes

REGISTER >>

COMSOL

## Lasing behaviors upon phase transition in solution-processed perovskite thin films

Tsung Sheng Kao, Yu-Hsun Chou, Chun-Hsien Chou, Fang-Chung Chen,<sup>a)</sup>  
 and Tien-Chang Lu<sup>a)</sup>

*Department of Photonics and Institute of Electro-Optical Engineering, National Chiao Tung University,  
 Hsinchu 30010, Taiwan*

(Received 13 October 2014; accepted 28 November 2014; published online 9 December 2014)

In this paper, the temperature dependent lasing characteristics of solution-processed organic-inorganic halide perovskite  $\text{CH}_3\text{NH}_3\text{PbI}_3$  films have been demonstrated. The lasing temperature can be sustained up to a near room temperature at 260 K. Via the temperature dependent photoluminescence (PL) measurements, an emerged phase-transition band can be observed, ascribing to the crystalline structures changed from the orthorhombic to tetragonal phase states in the perovskites as a function of a gradual increase in the ambient temperature. The optical characteristics of the PL emission peaks and the anomalous shifts of the peak intensities are highly correspondent with the phase states in perovskites at different temperatures, showing a low-threshold lasing behavior at the phase transition. The laser cavities may be formed under multiple random scattering provided by the polycrystalline grain boundary and/or phase separation upon the phase transition. Since the threshold gain is potentially high in the random cavities, the large material gain exhibited by the solution-processed perovskite would be very promising in making practical laser devices. © 2014 AIP Publishing LLC. [<http://dx.doi.org/10.1063/1.4903877>]

Solution processable optoelectronic materials are fascinated for their great capabilities in the cost-effective and large-scale manufacturing in optoelectronics devices. Among the tremendous research efforts conducted during in the last 2 years, the hybrid organic-inorganic metal-halide perovskites now show the photovoltaic power conversion efficiency approaching 18% and long-range balanced electron-hole transport distances.<sup>1–6</sup> More interestingly, the solution-processed perovskite films recently have shown promising photoluminescence (PL) quantum efficiencies exceeding 70% and the wavelength-tunable lasing performance in hybrid perovskite films with different halides, making them a promising candidate for the applications in efficient light emitting diodes (LEDs) and on-chip coherent light sources.<sup>7,8</sup> Therefore, numerous studies, which focused on the excitonic properties, recombination lifetimes, optical absorbance, and carrier mobilities, have been made to investigate the specific material properties in the perovskite films, revealing the optoelectronic processes accompanied with established theoretical models.<sup>9–16</sup>

Hybrid organic-inorganic perovskites are intrinsically complex materials. The existence of various crystalline structures or phase states at different ambient temperatures may cause intricate interactions between structural disorders, resulting in different materials properties and optical characteristics. From the previous experiments and theoretical studies,<sup>17–23</sup> the fundamental  $\text{CH}_3\text{NH}_3\text{PbX}_3$  (X: Cr, Br, or I) halide structures are basically built of the organic  $(\text{CH}_3\text{NH}_3)^+$  cation and  $(\text{PbX}_3)^-$  inorganic anion. The versatility of the organic part affords the possibility of fine tuning material properties, thus affecting the optical performance of

different perovskites. For example, the optical spectra of engineered lead halide organic-inorganic perovskites can be easily tailored by varying the organic cation, giving a great improvement of the optical efficiencies and fine tuning of the emission wavelengths.<sup>24</sup> Also, self-assembled layered perovskite structures have recently shown enhanced nonlinear optical properties in microcavities.<sup>25</sup> In this paper, we investigate the relation between the phase-transition of the perovskite thin films and the lasing mechanism at different phase states. It may provide further studies on the perspectives of future lasing and lighting industries.

To prepare the solution-processed organic-inorganic halide perovskite thin films, lead iodide ( $\text{PbI}_2$ , Sigma-Aldrich) was first dissolved completely in *N,N*-dimethylformamide (DMF) and the solution was kept stirring at 60 °C overnight inside a nitrogen-filled glove box. The weight percentage of  $\text{PbI}_2$  was controlled at 30 wt. %. For the fabrication of the perovskite films, the as-prepared  $\text{PbI}_2$  solution was first spin-coated on a 70 °C UV-cleaned glass substrate at 6000 rpm for 30 s, and the yellow  $\text{PbI}_2$  film was subsequently dried at 70 °C for 15 min as the diagram schematically described in Fig. 1(a). Next, the  $\text{PbI}_2$  film was covered with a 1 wt. % precursor solution of methylammonium iodide ( $\text{CH}_3\text{NH}_3\text{I}$ ) in 2-propanol (IPA) at room temperature. The IPA solution was gradually dried in 40 s and the sample was subject to a spin-coating process in order to remove the solvent completely. The resulting films were annealed at 100 °C for 2 h to form the dark-brown  $\text{CH}_3\text{NH}_3\text{PbI}_3$  perovskite layers of around 300 nm in thickness. By conducting the spectral measurement at room temperature, the ground state absorption spectrum of the fabricated perovskite thin films can be acquired as the result (blue line) demonstrated in Fig. 1(d), exhibiting an absorption edge of around 1.59 eV. Such an absorption edge is consistent with the previous reports and it may

<sup>a)</sup>Electronic addresses: fcchen@mail.nctu.edu.tw and timtclu@mail.nctu.edu.tw

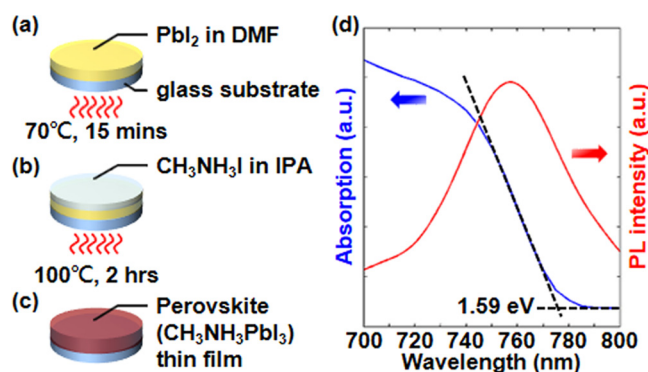


FIG. 1. Schematic diagram of the perovskite  $\text{CH}_3\text{NH}_3\text{PbI}_3$  films prepared in solution processes. (a) The yellow lead iodide  $\text{PbI}_2$  is dissolved in DMF solution and then dried using a hot-plate heating at  $70^\circ\text{C}$  for 15 min. (b) After dropping 1 wt.% methylammonium iodide  $\text{CH}_3\text{NH}_3\text{I}$  precursor onto the cooled  $\text{PbI}_2$  film, the  $\text{PbI}_2/\text{CH}_3\text{NH}_3\text{I}$  stacking films are heated at  $100^\circ\text{C}$  for 2 h to form dark-brown  $\text{CH}_3\text{NH}_3\text{PbI}_3$  perovskite layers as shown in (c). The thickness of the solution-processed perovskite films is about 300 nm. (d) Ground state absorption (blue) and PL emission (red) spectra of the fabricated perovskite thin film is measured at room temperature, indicating that the photon emission energy is close to the absorption edge of the perovskite films at around 1.59 eV.

attribute to the direct bandgap transition from the valence band maximum to the conduction band minimum in  $\text{CH}_3\text{NH}_3\text{PbI}_3$ .<sup>3,4,16,26</sup>

To investigate the coherent light emission properties at different crystalline phase states of the organic-inorganic halide perovskite thin films, the temperature-dependent PL measurements were conducted using a third harmonic generation (THG) of a  $\text{Nd:YVO}_4$  pulse laser as an optical excitation source of 355 nm, while the pulse duration and the repetition rate were 0.5 ns and 1 kHz, respectively. By launching the laser light beam into a microscope objective lens of 0.55 N.A., the focal spot size can be concentrated at around  $10\ \mu\text{m}$  in diameter, irradiating on the perovskite sample surface. Light emitted from the perovskites was collected by the same objective lens and transmitted through a UV optical fiber of an angular resolution of  $1^\circ$  into a monochromator (Horiba iHR320) with a spectral resolution of 0.2 nm together with a nitrogen cooled charge-coupled device (CCD), recording the PL emission spectra at different characteristic excitation powers and ambient temperatures. Figure 1(d) represents one of the measured PL spectra (red line) as the perovskite film was pumped with a weak optical excitation at room temperature (300 K), exhibiting a maximum intensity of the photon emission close to the absorption edge. Thus, the light emission behaviors in the phase transition of the perovskite thin films may be investigated and analyzed via a series of PL measurements conducted at different temperatures.

The temperature-dependent PL emission spectra of the fabricated organic-inorganic lead halide perovskite films are shown in Fig. 2, while the optical excitation is set at a low pumping power of  $100\ \mu\text{W}$  in order to thoroughly comprehend the phase transition in the perovskites in a broad temperature range. Regarding the PL measurements in a sequence of heating process from 77 K to 240 K, a sharp peak with the maximum spectral intensity occurs at the temperature of 120 K and the corresponding PL emission

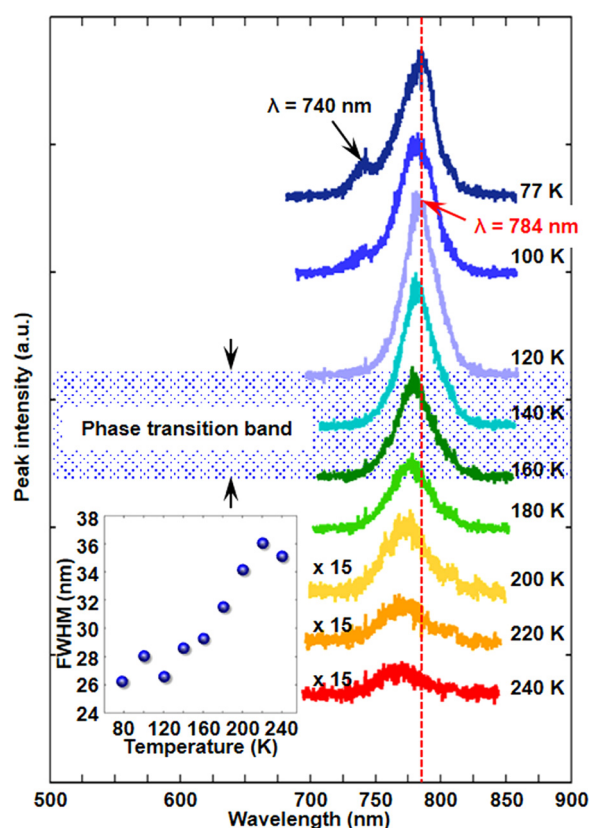


FIG. 2. Temperature-dependent PL measurements of the organic-inorganic halide perovskite films at a low optical pumping power of  $100\ \mu\text{W}$ . The temperature is varied in a range from 77 K to 240 K. In the PL measurements, the wavelength of a  $\text{Nd:YVO}_4$  pulse laser light source is 355 nm, and the spot size is focused by a microscope objective lens (N.A.:0.55,  $100\times$ ) at around  $10\ \mu\text{m}$  in diameter. The maximum photon emission intensity occurs at the temperature of 120 K, while the PL spectrum is centered at 784 nm. Above or below this characteristic temperature  $T_c$ , all the other PL emission spectra show a blue-shift tendency in their central wavelengths, indicating a distinguished phase transition band occurs in the range from 120 K to 160 K. The inset shows the corresponding emission linewidths of each PL emission peak.

spectrum is centered at 784 nm. Above or below this characteristic temperature  $T_c$ , all the other PL emission spectra show a blue-shift tendency on their central wavelengths, thus giving an obvious variation of the spectral characteristics in a range of temperatures from 120 K to 160 K as indicated in Fig. 2. Such a temperature range of the PL spectral behavior change may refer to a structural phase transition which occurs from an orthorhombic to a tetragonal crystalline structures during the temperature-increasing process.<sup>12,27–29</sup> This orthorhombic-to-tetragonal phase transition, accompanied by a tilting of the  $\text{PbI}_6$ -octahedra out of the  $ab$ -plane, has been observed in several temperature-dependent studies.<sup>28,29</sup>

At low temperatures around the characteristic temperature  $T_c$ , the PL emission peak at around 784 nm is attributed to the excitonic transition in the perovskites, while with a further reduction of temperature a second excitonic peak emerges at  $\sim 740\ \text{nm}$ .<sup>12</sup> This second excitonic peak indicates that two crystalline phases coexist, since our fabricated perovskite films are polycrystalline and may gain the strength in intensity as the temperature decreases to extremely low, whereas the first emission peak disappears. Above the



temperature  $T_c$ , the excitonic peak dramatically decreases with blue shifts of the spectral centers in the heating process towards to the room temperature. This phenomenon, as well as the anomalous Varshni trend observed in lead/copper composite semiconductors, may result from the interactions between the electron–phonon renormalization and the thermal expansion in perovskites when the ambient temperature increases.<sup>12,30,31</sup>

The perovskite films stated above also provide a significant light emission enhancement for lasing with a low threshold at around the temperature  $T_c$ . Figure 3(a) shows the lasing characteristics of the perovskite films in an optical excitation power range from  $10\ \mu\text{W}$  to  $1\ \text{mW}$  at the temperature of  $120\ \text{K}$ . Under low optical power excitation, only very broad spontaneous emission spectra can be observed at the spectral centers of around  $784\ \text{nm}$ . With a gradually increased pumping powers, the emission intensity increases dramatically as the excitation power exceeds  $250\ \mu\text{W}$ , while the emission peak appears at around  $800\ \text{nm}$  as represented in the inset figure. The energy difference between the lasing

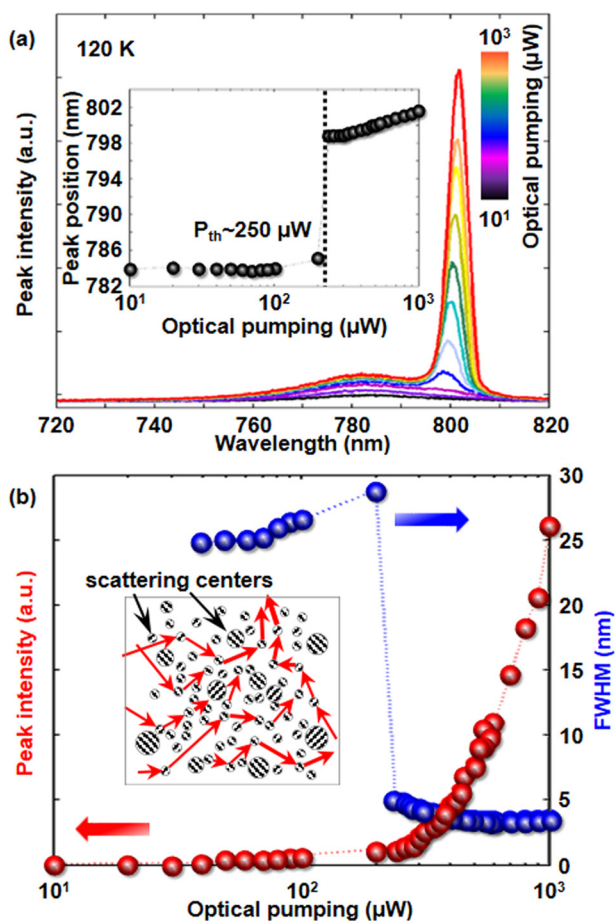


FIG. 3. Lasing characteristics of the perovskite films recorded as a function of optical pumping powers at the temperature of  $120\ \text{K}$ . (a) PL emission spectra of the fabricated perovskite films photo-excited at different optical pumping powers from  $10\ \mu\text{W}$  to  $1\ \text{mW}$ . The inset denotes the maximum photon emission energy at each PL measurement. (b) L-L curve (red) plotted in a log-linear scale and the corresponding linewidths (blue) as a function of incident optical pumping powers. A distinguished lasing behavior takes place at the threshold pumping power,  $P_{th}$ , of around  $250\ \mu\text{W}$ . The schematic draw depicts the proposed lasing mechanism via random scattering provided by the polycrystalline grain boundary and/or phase separation upon the phase transition.

and the spontaneous emission peaks is around  $30\ \text{meV}$ . Figure 3(b) shows the light-light (L-L) plot of the lasing mode and the significant reduction in corresponding linewidths at full width at half maximum (FWHM) of the peaks occurred at around  $800\ \text{nm}$ . Eventually, the FWHM drops down to about  $4\ \text{nm}$  from  $\sim 25\ \text{nm}$  as blue dots shown in Fig. 3(b). Both the results show a typical fingerprint for lasing and give an estimation of the threshold power at around  $250\ \mu\text{W}$ . Since there is no specifically defined laser cavities in these perovskite films, the optical feedback for lasing could be formed via random scattering provided by the polycrystalline grain boundary and/or phase separation upon the phase transition which may originate from the generated crystalline structures at different sizes and co-existing phase states randomly distributed in perovskite thin films.<sup>32–36</sup> The proposed lasing mechanism is schematically depicted as the inset shown in Fig. 3(b). The random scattering also facilitates stronger spontaneous emission intensity at the temperature of  $120\ \text{K}$ .

Regarding the lasing stability of the perovskite thin films modulated with time, the lasing characteristics measurements were conducted by keeping the perovskite films in a high-vacuum chamber, thus preventing the hydrolysis of the perovskite materials and maintaining the lasing stability for a longer period of time.

The lasing mechanism at low temperatures can be further explained as follows.<sup>28</sup> Since our fabricated organic-inorganic perovskite thin films are considered as polycrystalline structures, the tetragonal phase may coexist with the orthorhombic crystallites at different temperatures with various composition ratios. In the coexisting crystallographic phases, the tetragonal inclusions can trap more photo-excited carriers than the orthorhombic crystallites due to the lower conduction band in the tetragonal phases. Upon stronger excitation, the carrier density in tetragonal crystallites may saturate and a significant number of carriers may recombine within the orthorhombic phase, hence causing substantial emission at the correspondingly higher energy and thus slight spectral blue-shifts before the lasing starts. The presumption of the coexisting states may also indicate that the carrier density and the number of the tetragonal phase are at an equilibrium state at the temperature of  $120\ \text{K}$ , giving the lowest power threshold for lasing as indicated in Fig. 4(a). Upon the further reduction of temperature, more orthorhombic phases were generated in perovskite thin films, causing a higher power threshold. Furthermore, under weak excitation, the low number of initially free carriers may just partially fill the sub-gap distribution of states in the tetragonal crystallites, giving a broadened and downshifted emission observed from the PL emission spectra.

As the temperature exceeds  $120\ \text{K}$ , the lasing threshold continues to increase because of the thermal broadening of gain peak, which is similar to the conventional lasing behavior. Figure 4(b) represents the peak position difference (detuning) between the lasing mode and the spontaneous emission of the organic-inorganic perovskites at different temperatures. The detuning originates from the balance between absorption spectra of the perovskite thin films and light amplification spectra formed by the random cavities. As the results shown in the figure, the spectral peak positions of the spontaneous emission are quite close to the lasing

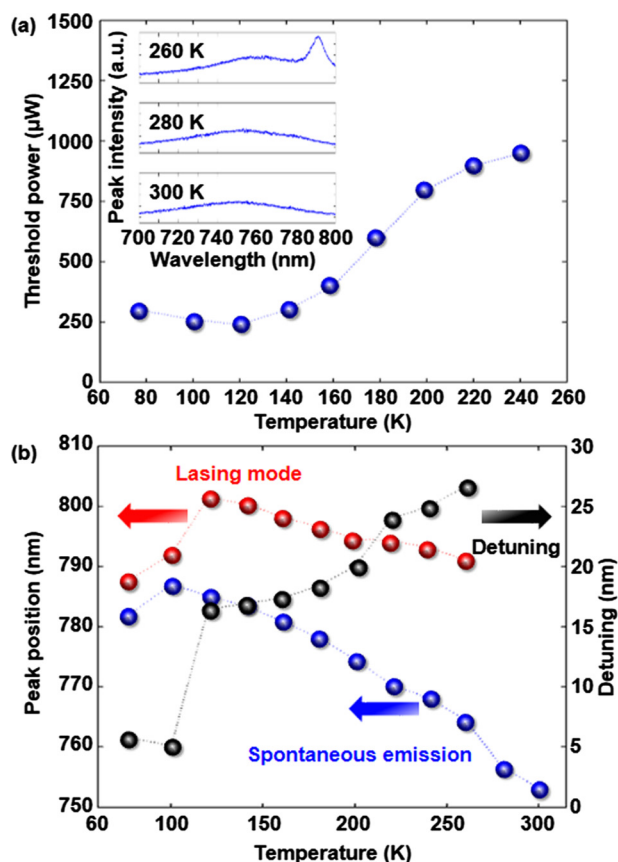


FIG. 4. Temperature-dependent lasing behaviors. (a) Lasing threshold power of the perovskite thin films in a temperature range from 77 K to 240 K. Above 260 K, less lasing behavior can be observed even the excitation power is larger than 5 mW as the PL results shown in the inset. (b) The wavelength difference (detuning) between the lasing and the spontaneous emission peaks at different temperatures.

peaks as the temperature is lower than the characteristic temperature  $T_c$ . With an increase of the ambient temperature, the emission wavelength of the lasing mode slightly shifts 10 nm in a broad temperature range, while the spontaneous emission shows a dramatic change from 787 nm to 753 nm, corresponding an energy difference of about 70 meV. The increasing detuning value could be the results of broadening absorption edge as the temperature is elevated, which pushes the lasing peak away from the spontaneous emission peak. This increasing detuning value agrees well to the linewidth broadening of spontaneous emission shown in the inset of Fig. 2. The lasing characteristics we can observe is up to a near room temperature of 260 K as shown in the inset of Fig. 4(a). Although the perovskite films exhibit inherent instability in their compositions under UV illumination,<sup>37</sup> we may expect that the low threshold perovskite lasers still can be accomplished and operated at room temperature, since the well-defined resonant cavity is formed. Moreover, the better lasing performance can be acquired once we use a pumping source in the visible wavelength range.

In summary, we have investigated the temperature dependent photoluminescence emission from the organic-inorganic halide perovskite  $\text{CH}_3\text{NH}_3\text{PbI}_3$  thin films which were synthesized via a relatively simple solution process in fabrications. A phase-transition band can be located, ascribing to orthorhombic-to-tetragonal phase transition in the

perovskites within a heating process from low to high temperature. The optical characteristics of the PL emission peaks and the anomalous shifts of the peak intensities are highly correspondent with the phase states in perovskites at different ambient temperatures. In addition, we have demonstrated the temperature dependent lasing characteristics, while the lasing temperature can be sustained up to 260 K. The carrier trapping and photon scattering are significantly influenced by the phase transition and in turn result in anomalous lasing characteristics. On the other hand, the relative large optical gain bearing the random lasing in the solution-processed perovskite thin films indicates that the efficient and cost-effective coherent light sources can be implemented in the near future.

We acknowledge the help of Professor S. C. Wang and Professor H. C. Kuo at National Chiao Tung University for contributing fruitful discussions and technical support. This work was partially supported by the Ministry of Education Aim for the Top University program and by the Ministry of Science and Technology of Taiwan under Contract Nos. NSC 102-2221-E-009-156-MY3 and NSC 101-2628-E-009-008-MY3.

<sup>1</sup>M. A. Green, A. Ho-Baillie, and H. J. Snaith, *Nature Photon.* **8**, 506 (2014).

<sup>2</sup>C. Wehrenfennig, G. E. Eperon, M. B. Johnston, H. J. Snaith, and L. M. Herz, *Adv. Mater.* **26**, 1584 (2014).

<sup>3</sup>S. D. Stranks, G. E. Eperon, G. Grancini, C. Menelaou, M. J. P. Alcocer, T. Leijtens, L. M. Herz, A. Petrozza, and H. J. Snaith, *Science* **342**, 341 (2013).

<sup>4</sup>G. Xing, N. Mathews, S. Sun, S. S. Lim, Y. M. Lam, M. Gratzel, S. Mhaisalkar, and T. C. Sum, *Science* **342**, 344 (2013).

<sup>5</sup>A. Sadhanala, F. Deschler, T. H. Thomas, S. E. Dutton, K. C. Goedel, F. C. Hanusch, M. L. Lai, U. Steiner, T. Bein, P. Docampo, D. Cahen, and R. H. Friend, *J. Phys. Chem. Lett.* **5**, 2501 (2014).

<sup>6</sup>H. Zhou, Q. Chen, G. Li, S. Luo, T.-B. Song, H.-S. Duan, Z. Hong, J. You, Y. Liu, and Y. Yang, *Science* **345**, 542 (2014).

<sup>7</sup>G. Xing, N. Mathews, S. S. Lim, N. Yantara, X. Liu, D. Sabba, M. Gratzel, S. Mhaisalkar, and T. C. Sum, *Nature Mater.* **13**, 476 (2014).

<sup>8</sup>F. Deschler, M. Price, S. Pathak, L. E. Klintberg, D.-D. Jarausch, R. Higler, S. Hüttner, T. Leijtens, S. D. Stranks, H. J. Snaith, M. Atatüre, R. T. Phillips, and R. H. Friend, *J. Phys. Chem. Lett.* **5**, 1421 (2014).

<sup>9</sup>C. S. Ponseca, T. J. Savenije, M. Abdellah, K. Zheng, A. Yartsev, T. Pascher, T. Harlang, P. Chabera, T. Pullerits, A. Stepanov, J.-P. Wolf, and V. Sundström, *J. Am. Chem. Soc.* **136**, 5189 (2014).

<sup>10</sup>A. Marchioro, J. Teuscher, D. Friedrich, M. Kunst, R. van de Krol, T. Moehl, M. Gratzel, and J.-E. Moser, *Nature Photon.* **8**, 250 (2014).

<sup>11</sup>S. Sun, T. Salim, N. Mathews, M. Duchamp, C. Boothroyd, G. Xing, T. C. Sum, and Y. M. Lam, *Energy Environ. Sci.* **7**, 399 (2014).

<sup>12</sup>V. D'Innocenzo, G. Grancini, M. J. P. Alcocer, A. R. S. Kandada, S. D. Stranks, M. M. Lee, G. Lanzani, H. J. Snaith, and A. Petrozza, *Nat. Commun.* **5**, 3586 (2014).

<sup>13</sup>C. Wehrenfennig, M. Liu, H. J. Snaith, M. B. Johnston, and L. M. Herz, *J. Phys. Chem. Lett.* **5**, 1300 (2014).

<sup>14</sup>J. H. Noh, S. H. Im, J. H. Heo, T. N. Mandal, and S. I. Seok, *Nano Lett.* **13**, 1764 (2013).

<sup>15</sup>G. E. Eperon, S. D. Stranks, C. Menelaou, M. B. Johnston, L. M. Herz, and H. J. Snaith, *Energy Environ. Sci.* **7**, 982 (2014).

<sup>16</sup>J. S. Manser and P. V. Kamat, *Nature Photon.* **8**, 737 (2014).

<sup>17</sup>J. Even, L. Pedesseau, J.-M. Jancu, and C. Katan, *J. Phys. Chem. Lett.* **4**, 2999 (2013).

<sup>18</sup>Y. Kawamura, H. Mashiyama, and K. Hasebe, *J. Phys. Soc. Jpn.* **71**, 1694 (2002).

<sup>19</sup>C. Quarti, G. Grancini, E. Mosconi, P. Bruno, J. M. Ball, M. M. Lee, H. J. Snaith, A. Petrozza, and F. De Angelis, *J. Phys. Chem. Lett.* **5**, 279 (2014).

<sup>20</sup>J. Feng and B. Xiao, *J. Phys. Chem. Lett.* **5**, 1278 (2014).

<sup>21</sup>W. Geng, L. Zhang, Y.-N. Zhang, W.-M. Lau, and L.-M. Liu, *J. Phys. Chem. C* **118**, 19565 (2014).

- <sup>22</sup>X. Zhu, H. Su, R. A. Marcus, and M. E. Michel-Beyerle, *J. Phys. Chem. Lett.* **5**, 3061 (2014).
- <sup>23</sup>J. Haruyama, K. Sodeyama, L. Han, and Y. Tateyama, *J. Phys. Chem. Lett.* **5**, 2903 (2014).
- <sup>24</sup>D. B. Mitzi, S. Wang, C. A. Feild, C. A. Chess, and A. M. Guloy, *Science* **267**, 1473 (1995).
- <sup>25</sup>Y. Wei, J. S. Lauret, L. Galmiche, P. Audebert, and E. Deleporte, *Opt. Express* **20**, 10399 (2012).
- <sup>26</sup>J. Even, L. Pedesseau, and C. Katan, *J. Phys. Chem. C* **118**, 11566 (2014).
- <sup>27</sup>T. Baikie, Y. Fang, J. M. Kadro, M. Schreyer, F. Wei, S. G. Mhaisalkar, M. Graetzel, and T. J. White, *J. Mater. Chem. A* **1**, 5628 (2013).
- <sup>28</sup>C. Wehrenfennig, M. Liu, H. J. Snaith, M. B. Johnston, and L. M. Herz, *APL Mater.* **2**, 081513 (2014).
- <sup>29</sup>A. Poglitsch and D. Weber, *J. Chem. Phys.* **87**, 6373 (1987).
- <sup>30</sup>Y. P. Varshni, *Physica* **34**, 149 (1967).
- <sup>31</sup>K. Wu, A. Bera, C. Ma, Y. Du, Y. Yang, L. Li, and T. Wu, *Phys. Chem. Chem. Phys.* **16**, 22476 (2014).
- <sup>32</sup>H. Cao, Y. G. Zhao, H. C. Ong, S. T. Ho, J. Y. Dai, J. Y. Wu, and R. P. H. Chang, *Appl. Phys. Lett.* **73**, 3656 (1998).
- <sup>33</sup>X. Liu, A. Yamilov, X. Wu, J.-G. Zheng, H. Cao, and R. P. H. Chang, *Chem. Mater.* **16**, 5414 (2004).
- <sup>34</sup>H. D. Li, S. F. Yu, S. P. Lau, and E. S. P. Leong, *Appl. Phys. Lett.* **89**, 021110 (2006).
- <sup>35</sup>J. Fallert, R. J. B. Dietz, J. Sartor, D. Schneider, C. Klingshirn, and H. Kalt, *Nature Photon.* **3**, 279 (2009).
- <sup>36</sup>D. Wiersma, *Nature* **406**, 132 (2000).
- <sup>37</sup>T. Leijtens, G. E. Eperon, S. Pathak, A. Abate, M. M. Lee, and H. J. Snaith, *Nat. Commun.* **4**, 2885 (2013).